Local Order Refinement in Liquid Lithium Niobate Using a Two Radiation Method (X-Rays and Neutrons)

P. Andonov [1], P. Chieux [2], S. Kimura [3], and Y. Waseda [4]

[1] Laboratoire de Magnétisme et Matériaux Magnétiques de Bellevue, 1, place Aristide Briand, 92195 Meudon Cedex, France
[2] Institut Laue-Langevin 156 X centre de tri 38042 Grenoble, France
[3] National Institute for Research in Inorganic Materials (NIRIM), I-I Namiki, Tsukuba Ibaraki, 305 Japan
[4] Institute for Advanced Materials Processing, Tohoku University, Sendaï, 980 Japan

Z. Naturforsch. **48a**, 955–964 (1993); received July 24, 1993

In the molten $LiNbO_3$, the local order of the first neighbouring atoms has been described using the total structure factors $S(Q)_{(x)}$ and $S(Q)_{(n)}$ and the total pair correlation functions $G(r)_{(x)}$ and $G(r)_{(n)}$ obtained by X-ray and neutron scattering, respectively. We have also compared the differences $[RDF(r)_{(x)} - RDF(r)_{(n)}]$ of the radial distributions obtained from experiments and computed from the distances in the $LiNbO_3$ crystal. With this refinement it was possible to extract the first pair distances $r_{1,Nb-O}$, $r_{1,Li-O}$ and $r_{1,O-O}$ with the high accuracy $\Delta r/r \approx 0.5\%$. These values are identical with those in the crystal. Fitting the RDF curves by Gaussian components centred around these distances, the first coordination numbers, $n_{1,Nb-O}$, $n_{1,Li-O}$ and $n_{1,O-O}$, have been determined with an accuracy $\Delta n/n \approx 2\%$. Octahedrally coordinated niobium atoms are present in the melt in the studied range from 1623 K to 1490 K. From these results it is inferred that aggregates built from corner-sharing octahedra, tightened by lithium atoms, are present in the melt.

I. Introduction

Lithium metaniobate $LiNbO_3$ is an interesting material owing to its electro-optical and non-linear optical properties [1, 2]. However the $LiNbO_3$ crystals are little used because of local fluctuations of the refractive index and the presence of many light scattering centers, defects caused probably by sub-grain boundaries [3–6]. Since both large and good quality crystals are needed for various optical devices, the production of sub-grain free crystals is required. As the monocrystals are produced by Czochralski's method of pulling from the melt, the local order in the liquid plays an important role in the crystallization process; therefore various structure-sensitive properties of the melt, such as viscosity, density and surface tension have been measured in order to find the best conditions for crystal growth [7–9]. A marked increase of the viscosity was always found at temperatures below 1555 K, and an anomalous variation, characteristic of a dilatant fluid, was also observed in the temperature range from 1560 K to 1590 K. These observations imply that there exist structural units or strong interactions in the liquid reinforcing the local ordering of the niobium oxide and lithium oxide and their mutual interactions at temperatures below 1555 K.

The $LiNbO_3$ crystal belongs to the family of ilmenites and its structure, resolved in the ferroelectric phase [10], belongs to the rhombohedral system with the space group R3c. The small Li atom is surrounded by a framework of eight octahedra of oxygen atoms, and a Nb atom is located at the center of each octahedron (Figure 1 a). It has been proposed that the space group becomes $R\bar{3}$ at the Curie point T_c, just a few degrees below the melting point $T_m \approx 1526$ K, but the structure of the paraelectric phase has not been resolved and T_c is not accurately known: $1415\ K \leq T_c \leq 1483\ K$ [10–14]. With Nb midway between nearest oxygen layers and Li in the oxygen layer c/4 from Nb, the position of the niobium atom has the symmetry of an inversion center in the paraelectric phase (Figure 1 b). The thermal expansion of the atomic bonds was studied by Megaw [15] and compared to those of other niobates belonging to the perovskite-family.

A cluster formation just above the melting point may be related to the appearance of sub-grain boundaries in the single crystal synthesis. With this in mind, recent structural studies of the $LiNbO_3$ melt have been carried out by means of small angle scatter-

Reprint requests to P. Andonov, Laboratoire de Magnétisme et Matériaux Magnétiques de Bellevue, 1, place Aristide Briand, 92195 Meudon Cedex, France.

0932-0784 / 93 / 1000-0955 $ 01.30/0. – Please order a reprint rather than making your own copy.

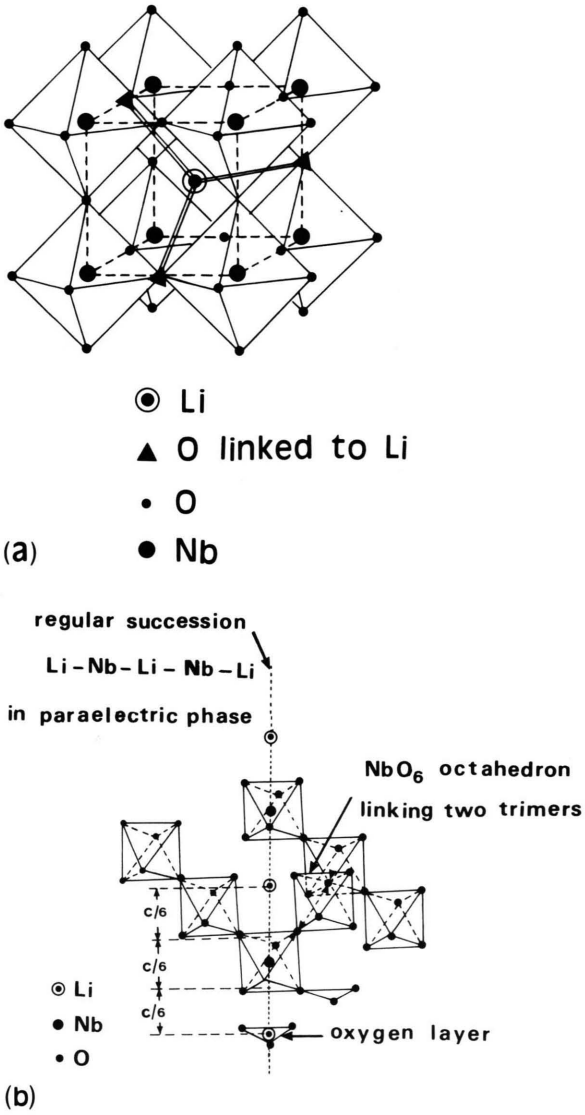

Fig. 1. Crystalline distribution. a) Regular framework of eight octahedra of oxygen atoms, b) regular succession of Li and Nb atoms in the paraelectric phase.

ing using synchrotron radiation [16] and by means of the high temperature diffraction method with X-rays [17] and neutrons [18]. Six experiments with different contributions W_{ij} of the i–j pairs are necessary to extract the $S_{ij}(Q)$ functions which determine the local order. Nevertheless, it is possible to obtain the first interatomic distances $r_{1,\mathrm{Nb-O}}$, $r_{1,\mathrm{Li-O}}$ and $r_{1,\mathrm{O-O}}$ using only the two total structure factors $S(Q)_{(x)}$ and $S(Q)_{(n)}$ and the two total radial distributions $\mathrm{RDF}(r)_{(x)}$ and $\mathrm{RDF}(r)_{(n)}$, owing to the large difference in the weights W_{ij} of both radiations in the case of the $LiNbO_3$ melt.

In this paper we report the results obtained by the comparison of the experimental difference $[\mathrm{RDF}(r)_{(x)} - \mathrm{RDF}(r)_{(n)}]$ with the difference computed from the interatomic distances observed in the rhombohedral phase. Using this refinement method, the i–j pairs have been identified and their interatomic distances have been determined with a good accuracy for the first neighbour atoms. A local ordering, similar to the crystalline local order, has been confirmed.

II. Experimental

The experiments are described in [17, 18]; here we only recall the ranges of the temperature (T) and wave vector (Q) explored with both radiations.

The neutron experiments were carried out on the D4B spectrometer at the Institute Laue-Langevin in Grenoble. With the angular range of the measurement maintained within $1.6° \leq 2\Theta \leq 131.4°$ (2Θ = scattering angle) and the wavelength $\lambda = 0.7064$ Å, $Q = (4\pi \sin\Theta)/\lambda$ is investigated from $0.27\,\text{Å}^{-1}$ to $16.26\,\text{Å}^{-1}$. The counting accuracy is always better than 0.2%, i.e. such that the statistical errors were always small as compared to the effects induced by temperature variations. The intensities $I_s(2\Theta)$, scattered by the melt, were measured at sixteen values of T, T decreasing by steps from 1623 K to 1490 K. A large undercooling domain was observed ($\Delta T \approx 36°$), the onset of crystallization having been detected only below 1490 K, where Bragg peaks appeared. The total interference function was obtained using the procedure described in [19]. The intensities were corrected for background, furnace and cell scattering, and sample self-absorption using the values of the scattering and absorption cross sections of the three elements as listed in Table 1 [20, 21]. Multiple scattering, incoherent and inelastic scattering were subtracted. Then, the normalization to the known scattering cross section was achieved in the high Q-domain where the oscillations of the scattered intensities were small.

Following the evolution of the first Bragg peak of $LiNbO_3$ crystal in situ during the initial temperature rise in the neutron diffraction study [18], and assuming an isotropic continuous expansion in the rhombohedral phase, it was possible to determine an approximate mean expansion coefficient $\alpha_m \approx 3.3 \times 10^{-5}$ per degree.

Table 1. Coherent cross-section and linear total absorption coefficient of the various materials.

	Lithium	Niobium	Oxygen
b_{coh} (10^{-12} cm)	−1.903	5.805	7.054
μ_{total}	$LiNbO_3$ at 1540 K ⇒		0.721_6 cm^{-1}
	Platinum ⇒		1.047_5 cm^{-1}
	Vanadium ⇒		0.518_9 cm^{-1}

The X-ray experiments were carried out on the diffractometer "theta-theta" at the University of Sendaï (SENKEN). With $2° \leq \Theta \leq 50°$ and the wavelength λ_{Mo}, Q is investigated from 0.6 Å^{-1} to 13.5 Å^{-1}. The $I_s(2\Theta)$ intensities were measured at three temperatures: 1548 K, 1573 K and 1598 K. The method of analyzing the X-ray scattering intensity is well established [22]. In order to convert the measured scattering intensity data into the coherent scattering intensity $I_{eu}^{coh}(Q)$ in electron units, the generalized Krogh-Moe-Norman method [23] was used with atomic formfactors including the anomalous dispersion corrections [24]. The Compton scattering was corrected using the values reported by Smith et al. [25].

For the X-ray experiments, the material was single crystal flakes of $LiNbO_3$ provided by Mitsui Mining and Smelting Co. Ltd.; the dimensions of these flakes were large enough to obtain, after melting, a large free horizontal surface of the melt. For the neutron experiments, the samples were prepared in the NIRIM at Tsukuba. Starting material was sintered $LiNbO_3$: Li_2CO_3 and Nb_2O_5 powders of high purity (99.99%) and natural isotopic abundance were mixed in congruent composition [26], pressed into a cylindrical form and calcined at 1000 °C for 5 hours. The final rods so-obtained are identical to those used for the growth of $LiNbO_3$ single crystals by the rf-heated Czochralski method. In view of the high corrosiveness of liquid $LiNbO_3$, the solid rod was introduced in a sealed platinum container and maintained under an oxidizing air atmosphere.

III. Data Processing

The method for analysing the scattering intensity of non-crystalline systems is now well established. Only a few additional details particular to this work are recalled below. Using the formalism of Faber and Ziman [27] generalized to a non-crystalline system including more than two kinds of atoms, the total structure factor $S(Q)$ can be related to the partial structure factors and the coherent scattering cross-section per atom $d\sigma_{coh}(Q)/d\Omega$ as follows:

$$S(Q) = \left\{ \frac{d\sigma_{coh}(Q)}{d\Omega} - \langle b^2 \rangle - \langle b \rangle^2 \right\} \Big/ \langle b \rangle^2 = \sum_{i=1}^{m} \sum_{j=1}^{m} W_{ij} S_{ij}(Q) . \quad (1)$$

In our case $m = 3$ and 1, 2, or 3 stand for Li, Nb, or O, respectively. More explicitly, (1) can be written as

$$S(Q) = \frac{c_1^2 b_1^2}{\langle b \rangle^2} S_{11}(Q) + \frac{c_2^2 b_2^2}{\langle b \rangle^2} S_{22}(Q) + \frac{c_3^2 b_3^2}{\langle b \rangle^2} S_{33}(Q) + \frac{2 c_1 c_2 b_1 b_2}{\langle b \rangle^2} S_{12}(Q) + \frac{2 c_2 c_3 b_2 b_3}{\langle b \rangle^2} S_{23}(Q) + \frac{2 c_3 c_1 b_3 b_1}{\langle b \rangle^2} S_{31}(Q) , \quad (2)$$

where

$$\langle b \rangle = \sum_{i=1,2,3}^{m} c_i b_i , \quad \langle b^2 \rangle = \sum_{i=1,2,3}^{m} c_i b_i^2$$

are the average coherent scattering length and the mean square of the scattering length, respectively; c_i and b_i are the atomic concentration and the coherent scattering length of element i, respectively, and W_{ij} is the pair cxontribution of the i, j pair or the weight of the partial structure factor S_{ij}.

The pair correlation function, $G(r)$, is obtained by a Fourier transformation to real space of the reduced function:

$$G(r) = \frac{2}{\pi} \int_{Q_{min}}^{Q_{max}} Q \cdot \{S(Q) - 1\} \cdot \sin(Qr) \cdot dQ , \quad (3)$$

which gives the radial distribution function:

$$RDF(r) = 4\pi r^2 \varrho_0 + r\, G(r) = 4\pi r^2 \varrho(r) , \quad (4)$$

where ϱ_0 is the average number density of atoms expressed in atoms · Å^{-3} and $\varrho(r)$ is the average radial density function.

The same formulas are applied to the X-ray diffraction with

$$4\pi r^2 \varrho(r) = 4\pi r^2 \varrho_0 + \frac{2r}{\pi} \int_0^{\infty} Q \frac{[I_{eu}^{coh}(Q) - \langle f(Q)^2 \rangle]}{\langle f(Q) \rangle^2} \sin(Qr)\, dQ . \quad (5)$$

Table 2. Weights (expressed in %) of the partial functions defined in (2) for neutron and X-ray scattering, respectively. In the latter case the W_{ij} values are reported for the Q-limits.

Pairs	W_{ij} (%)			Deviation $\Delta W_{ij} = W_{ij\,(\text{X-rays})} - W_{ij\,(\text{neutrons})}$
	Neutrons	X-rays		
		$Q=0$ Å^{-1}	13.5 Å^{-1}	
Li–Li	0.64	0.19	0.04	$-0.60 < \Delta W_{ij} < -0.46$
Nb–Nb	9.82	47.36	35.23	$25.41 - 37.55$
O–O	58.81	13.18	8.47	$-50.34 - -45.63$
Li–Nb	−5.03	5.16	2.87	$7.89 - 10.18$
Li–O	−12.30	3.15	1.21	$13.51 - 15.46$
Nb–O	48.05	43.09	40.05	$-8.00 - -4.96$

In this case $\langle f(Q)\rangle$ and $\langle f(Q)^2\rangle$ are the average scattering factor and the mean square of the atomic scattering factors, respectively, with $f_i(Q)$ depending on the wavevector Q.

The partial coordination numbers of atoms contained in the n-th shell are obtained by integration of the peaks of the partial radial distribution functions $\mathrm{RDF}_{ij}(r)$ as follows:

$$Z_{ij}^n = c_i \int_{r_{ij\,\min}^n}^{r_{ij\,\max}^n} \mathrm{RDF}_{ij}(r)\,\mathrm{d}r\,, \tag{6}$$

where $r_{ij\,\min}^n$ and $r_{ij\,\max}^n$ are the lower and upper limits of the n-th shell defined by the minima of RDF_{ij}; Z_{ij} is the average number of j-species atoms around any atom of type i, and the average distance between i and j atoms is given by $r_{ij} = \{r_{ij\,(\max)} + r_{ij\,(\min)}\} \cdot 1/2$ if the distribution can be approximated by a discrete Gaussian [28]. From global $\mathrm{RDF}(r)$ functions, the partial coordination numbers are determined using the same integration but applied to the resolved components of global peaks. The contributions W_{ij} of the i–j atomic pairs are calculated using the scattering lengths reported in Table 2 for the neutrons, and, for the X-rays the atomic form factors including anomalous dispersion corrections [23] or the analytic expressions of Cromer et al. [29, 30]. In neutron diffraction, the relative partial contributions of the different i–j pairs $W_{ij\,(n)}$ are constant in the whole Q-domain, but in X-ray diffraction each contribution varies with the form factor dependence on the wavevector. The values $W_{ij\,(x)}$ were calculated from $Q = 0$ Å^{-1} to $Q = 13.5$ Å^{-1} (limit reached in the X-rays study); the values $W_{ij\,(x)}$ and $W_{ij\,(n)}$ are reported in the Table 2 for the two extreme Q values with the ΔW_{ij} limits of the difference $\{W_{ij\,(x)} - W_{ij\,(n)}\}$. Due to the significant values observed for ΔW_{ij}, very important differences have to appear between the patterns showing either $S(Q)_{(x)}$ and $S(Q)_{(n)}$ or $\mathrm{RDF}(r)_{(x)}$ and $\mathrm{RDF}(r)_{(n)}$, extracted from the X-ray and neutron diffractions, respectively. Signs and absolute values of ΔW_{ij} will permit to identify the atomic species involved in the first neighbour pairs for which the mean interatomic distances are deduced from experimental $\mathrm{RDF}(r)$ functions. The comparison of these mean distances with the crystalline distances r_{ij} present in the rhombohedral phase is used to confirm the previous determination.

IV. Results

IV,1. General Observations

From the usual data analysis, after computation of $G(r)$ by Fourier transform of $Q\{S(Q)-1\}$ through (3) and $\mathrm{RDF}(r)$ through (4), the positions of well separated peaks may be defined with an accuracy $\Delta r/r \approx 1\%$, and the coordination numbers determined with an accuracy $\Delta n/n \approx 5\%$. When peaks have to be resolved into several components, the Gaussian distributions, usually used to represent the partial contributions, cannot be so accurately defined. Generally, we proceed by trial and error until an approximate fitting is observed. Width and position of Gaussian components can be altered and a unique solution is rarely obtained. Only partial distributions $G_{ij}(r)$, deduced from partial structure factors $S_{ij}(Q)$, enable the exact solution to be determined. But when only the global $S(Q)$ is available, atomic distributions have to be assumed. For instance in the case of the molten niobate, a first trial is made from the crystalline distances corrected for the estimated thermal expansion and regrouped to take the experimental resolution into account. The resultant mean distances give the positions of Gaussian components whose widths are adjusted to fit the global peak. But if another structure is assumed, with other components, another as good fit could possibly be obtained.

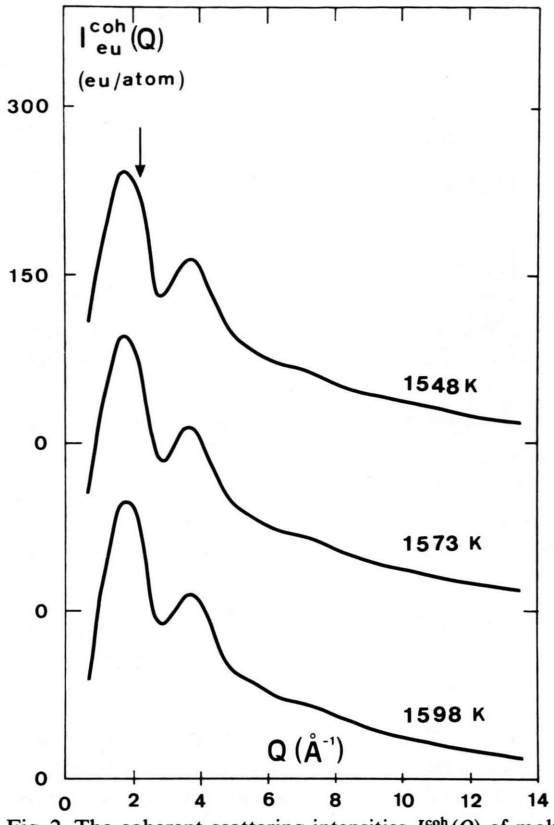

Fig. 2. The coherent scattering intensities $I^{coh}_{eu}(Q)$ of molten $LiNbO_3$ at 1548, 1573, and 1598 K. A shoulder at about $Q = 2.1$ Å^{-1}, denoted by an arrow, appears as T decreases towards T_m.

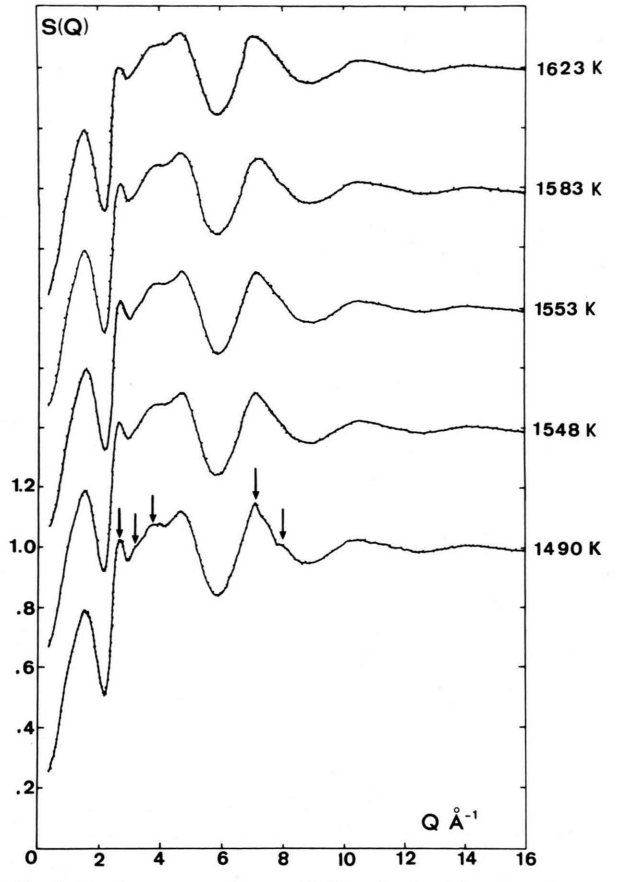

Fig. 3. Total structure factors $S(Q)_{(n)}$ obtained from neutron diffraction at different temperatures (the arrows indicate the most important changes).

No drastic change in the liquid structure of molten $LiNbO_3$ was evident from the X-ray diffraction data, obtained at 1598 K, 1573 K and 1548 K (Figure 2). In the case of neutrons with an explored T-range larger than the previous one, ($\Delta T \approx 133$ K, from 1623 K to 1490 K), the variation observed is also weak, see the $S(Q)_{(n)}$ factors shown in Fig. 3 (only five temperatures are displayed because no particular change was detected except in the undercooling domain; see small evolutions quoted by arrows in the more structured pattern at 1490 K). So, we present the method of refinement used in this data analysis for one temperature, $T = 1573$ K $\pm$ 10 K, chosen approximately at the middle of the different T ranges explored with X-rays and neutrons. The structure factors, $S(Q)_{(x)}$ and $S(Q)_{(n)}$, and the radial distribution functions, $RDF(r)_{(x)}$ and $RDF(r)_{(n)}$, obtained at 1573 K from both radiations, are shown in the Figs. 4 and 5, respectively.

IV,2. Determination of the r_{ij} Distances

To determine the mean r_{ij} distances in the melt and the type of atomic i–j pairs concerned at these distances, we compare the data obtained from both radiations. The experimental difference $\{RDF(r)_{(x)}\} - \{RDF(r)_{(n)}\}$ is shown in Figure 6a. The positions of the successive sharp maxima and minima give mean r values with an accuracy, ($\Delta r/r \approx 0.5\%$), better than the one obtained from the $RDF(r)$ curves. These r values are compared to the interatomic r_{ij} distances, computed from the atomic coordinates of the rhombohedral phase given at 300 K [10] and marked at the top of the Figure 6a. The arrows indi-

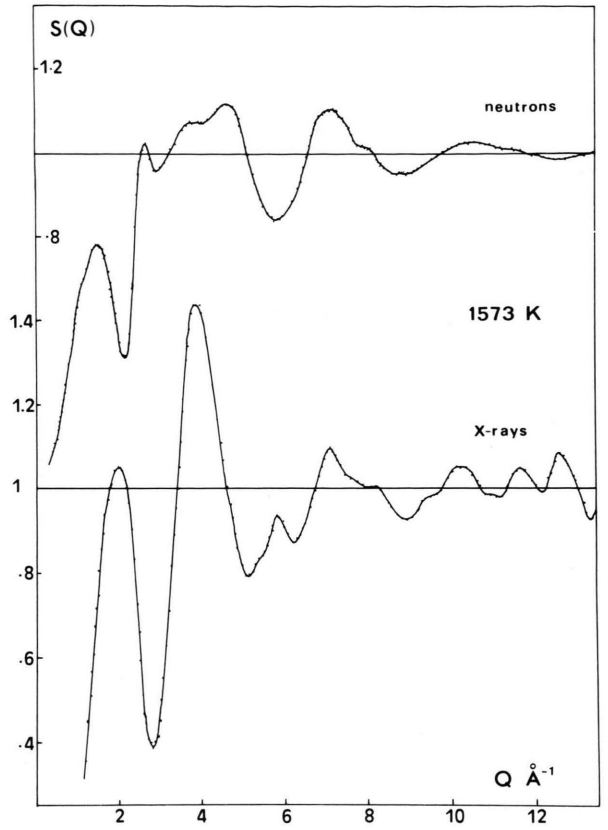

Fig. 4. Comparison of the total structure factors obtained at 1573 K from X-ray and neutron scattering, respectively.

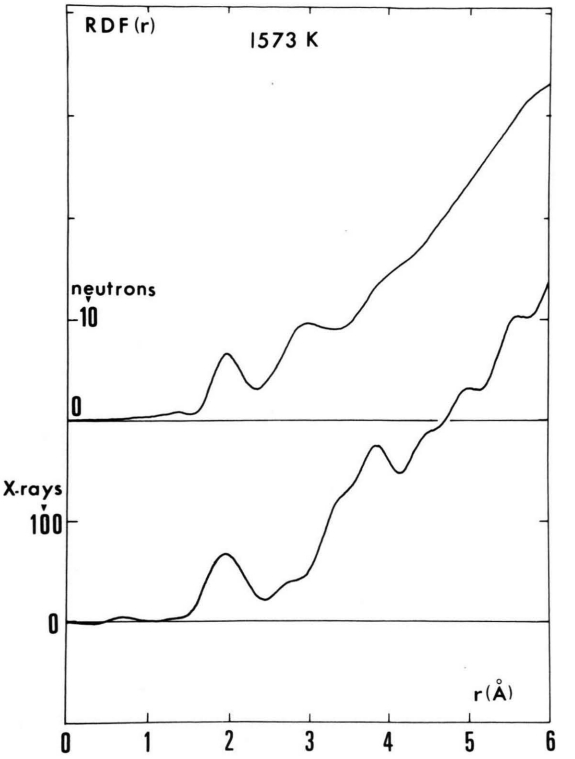

Fig. 5. Comparison of the total radial distributions obtained at 1573 K from X-ray and neutron scattering, respectively.

cate the mean values corresponding to the limit of resolution due to the Fourier transform, ($\Delta r \approx 0.3$ Å with $Q_{max} = 16$ Å^{-1}); values are quoted by arrows up or down according to whether the difference ΔW_{ij} relative to the $i-j$ pairs is positive or negative. A theoretical difference has been deduced from the theoretical distributions obtained as follows. For neutrons, the theoretical radial distribution, $[_{th}RDF(r)_{(n)}]$, was built using a Gaussian broadening of each peak of the distribution of the crystalline distances to take into account the limit of resolution (each r_{ij} distance is represented by a Gaussian having a FWHM $\Delta r =$ 0.3 Å and a height weighted by the value $W_{ij(n)}$ and the number of r_{ij} pairs). For X-rays, the theoretical radial distribution, $[_{th}RDF(r)_{(x)}]$, was not so easily obtained since $W_{ij(x)}$ depends on the Q value. We have built a first distribution, $[_{th1}RDF(r)_{(x)}]$, using the same Gaussian broadening as for neutrons and a height weighted by the constant mean value

$$[_cW_{ij(x)}] = 0.5 \times (W_{ij(x)_{Q=0}} + W_{ij(x)_{Q=13.5}}) \quad (7)$$

In a second method, a theoretical structure factor $_{th}S(Q)_{(x)}$ was computed using the theoretical intensity evaluated from the crystalline atomic coordinates and taking into account the variation of the atomic scattering factors, $f_i(Q)$, with the wavevector Q. In reciprocal space, the Dirac peaks, corresponding to the crystalline distribution, were replaced by Gaussian distributions to take the thermal fluctuations into account [31]. Then, after Fourier transformation to real space, we obtained the second theoretical radial distribution $[_{th2}RDF(r)_{(x)}]$. In the whole r-range used for the comparison, no important differences appeared between the two theoretical distributions. The theoretical difference $[_{th1}RDF(r)_{(x)} - _{th}RDF(r)_{(n)}]$ and the relative

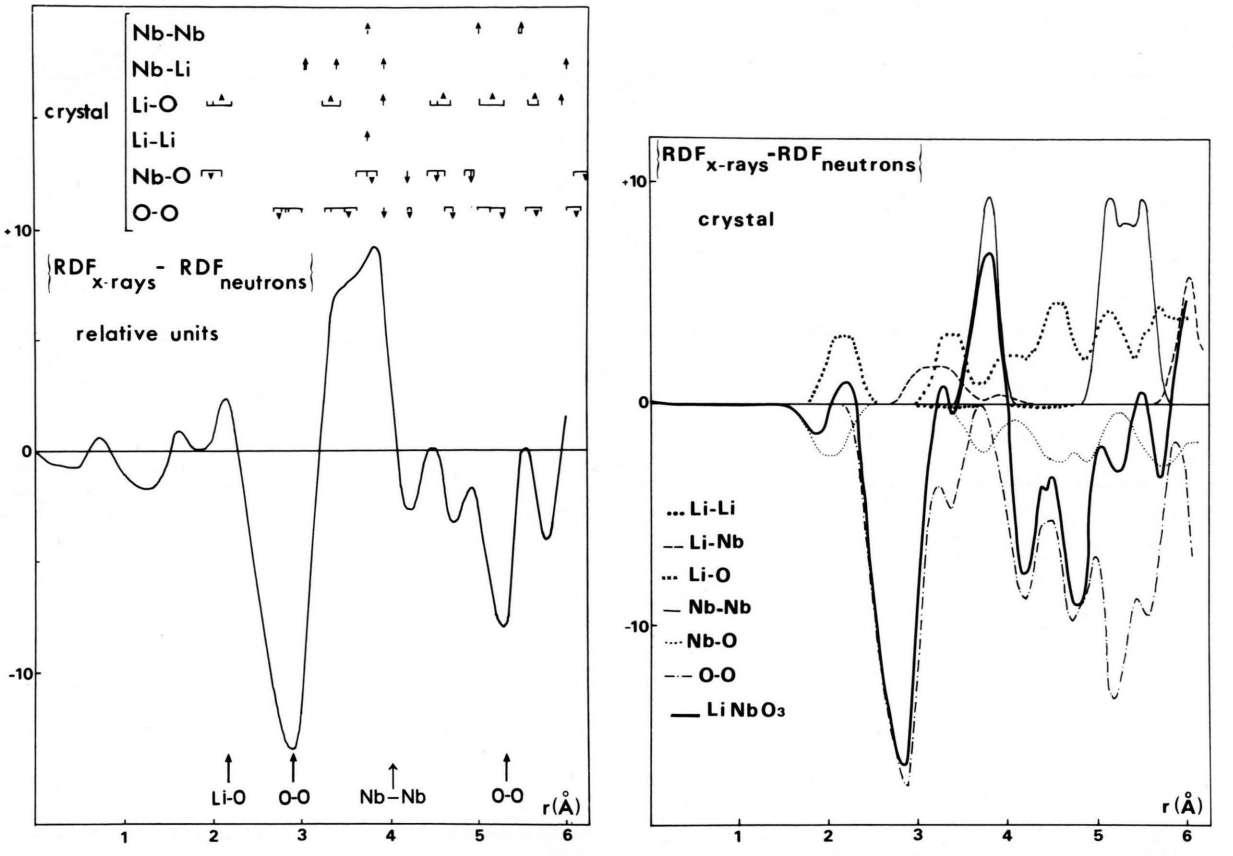

Fig. 6. Difference $\{RDF(r)_x\} - \{RDF(r)_n\}$. a) Experimental result obtained at 1573 K, b) theoretical evaluation from the crystalline distances at 300 K.

contributions due to each type of pair present in the $LiNbO_3$ crystal at 300 K are shown in Figure 6b.

The comparison of Figs. 6a and 6b shows that the first maximum, centred at $r_{ij} = 2.16 \pm 0.01$ Å, corresponds to a contribution of Li–O pairs only, and the large negative minimum, centred at $r_{ij} = 2.88 \pm 0.01$ Å, is explained by a contribution of O–O pairs only. Therefore the first distances $r_{1,\mathrm{Li-O}}$ and $r_{1,\mathrm{O-O}}$, are cofirmed in the liquid. The second positive oscillation and its left side shoulder are resolved into two main peaks for which the mean positions are given by the theoretical global curve. The first peak, centred around 3.45 Å, could be the sum of four superimposed contributions corresponding to the Li–Nb, Li–O, O–O and Li–Li pairs, the fourth one being negligible. None of these contributions can be confirmed. The second peak, centred around 3.82 Å, could be the sum of three superimposed contributions corresponding to the Li–O, Nb–O and Nb–Nb pairs, respectively; we have assumed this value for the first $r_{1,\mathrm{Nb-Nb}}$ distance in the melt since the Nb–Nb contribution is the most important one. The three successive negative deviations, observed at 4.22 Å, 4.72 Å, and 5.30 Å, are located at the positions of the negative maxima corresponding to contributions of the O–O pairs, but only the third distance can be attributed without doubt since in this r-range only one negative contribution, corresponding to the O–O pairs, exists. The last oscillation observed in Fig. 6a, centred around 5.51 Å, could be assigned to the Nb–Nb and Li–O pair contributions.

The arrows, drawn at the bottom of Fig. 6a, quote the four mean interatomic distances, r_{ij}, really confirmed by this comparative method: (1) $r_{1,\mathrm{Li-O}} \approx 2.16 \pm 0.01$ Å has to be compared with the distances in the crystal, $r_{\mathrm{Li-O}}$, between 2.0686 Å and 2.2386 Å with the mean value 2.1536 Å; (2) $r_{1,\mathrm{O-O}} \approx 2.88 \pm 0.01$ Å has to be compared with the crys-

talline distances, r_{O-O}, between 2,7190 Å and 2.8795 Å with a mean value 2.8564 Å; (3) $r_{1,Nb-Nb} \approx 3.82 \pm 0.02$ Å has to be compared with the crystalline distance, $r_{Nb-Nb} = 3.76$ Å and (4) $r_{O-O} \approx 5.30 \pm 0.03$ Å has to be compared with the crystalline distances r_{O-O} between 5.03 Å and 5.30 Å with the mean value 5.18 Å.

One other distance, $r_{1,Nb-O} \approx 1.94 \pm 0.04$ Å, has been determined from the $G(r)$ and RDF(r) curves using the usual method. Its value has to be compared with the crystalline distances between 1.8890 Å and 2.1124 Å with a mean value 2.00 Å.

IV,3. Determination of the n_{ij} Coordination Numbers

The low r-range of the experimental RDF$(r)_n$ curve is resolved with the first r_{ij} distances which have been defined (see Figure 7). The first peak is fitted with two Gaussian components whose mean scattering vectors, r_{ij}, and mean square deviations, $\sigma = \Delta r_{ij}^2$, are given in Table 3; $(\Delta r_{ij}^2)^{1/2}$ corresponds to the full width of the i–j pair distribution; its value is directly measured from the RDF peaks. If the local order in the liquid is similar to the crystalline one, the value of Δr_{ij} has to be about twice the maximal margin Δr_m observed between the corresponding crystalline r_{ij} distances. The first component is centred on the well separated first maximum located at $r_{1,Nb-O}$. The experimental value $\Delta r_{1,Nb-O} = 0.40$ Å agrees well with the value $2\Delta r_m \approx 2 \times 0.22$ Å. The second component is located at $r_{1,Li-O}$; and the value $\Delta r_{1,Li-O} \approx 0.38$ Å agrees well with $2\Delta r_m = 0.34$ Å. The second peak of the RDF(r) is not well separated; it is fitted by the component due to the O–O contribution centred at the distance $r_{1,O-O} \approx 2.88$ Å. Assuming a similitude between the liquid and crystalline local orders, no other contribution should be present in this r-range; so the maximal intensity of the component is given by the ordinate of RDF$(r)_{(n)}$ at $r = 2.88$ Å and its Δr value evaluated at half height after subtraction of the Li–O contribution. We obtain $\Delta_{1,O-O} = 0.80$ Å, a value barely superior to $\approx 2\Delta r_m$.

The corresponding coordination numbers are deduced from the respective areas of these components assuming that

$$n_{i-j} = \frac{c_j}{c_i} n_{j-i} \,. \tag{8}$$

The results, obtained at $T = 1573$ K using the above method, are reported in Table 3. At temperatures for which data are obtained from only one radiation, the usual analysis was applied, i.e., only the first RDF peak was processed and identified with Nb–O pairs. Very weak changes were observed in n_{Nb-O} ($5.94 \Rightarrow 6.03 \Rightarrow \approx 1.5\%$) and $r_{1,Nb-O}$ ($1.93_7 \Rightarrow 1.93_3 \Rightarrow \approx 0.3\%$) with T decreasing from 1623 K to 1490 K; these changes are smaller than the quoted experimental accuracies of the usual method ($\Delta n/n \approx 5\%$ and $\Delta r/r \approx 1\%$), see values reported in Table 4. We can write $r_{1,Nb-O} \approx 1.93_5 \pm 0.02$ Å and $n_{Nb-O} \approx 6.00 \pm 0.30$ in the studied T-range. The n_{Nb-O} coordination can be considered as constant and the Nb atom octahedrally coordinated as observed in the $LiNbO_3$ crystal.

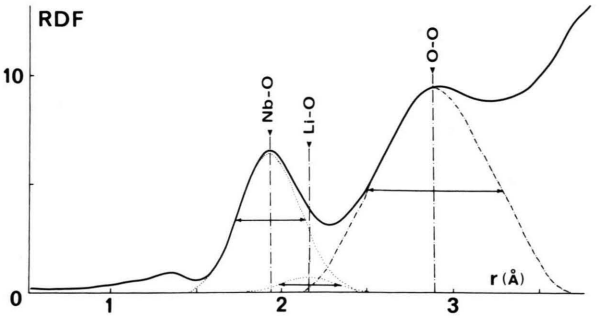

Fig. 7. Resolution of the first two peaks of RDF$(r)_{(n)}$ using the mean interatomic distances determined by the refinement method.

Table 3. Mean interatomic distances r_{ij} (Å) and mean square deviations σ (Å) used in the fit of the curve RDF$(r)_{(n)}$ at 1573 K.

Pairs i–j	r_{ij} (Å) ± 0.5%	σ (Å)	$n_{i-j} \pm 2\%$
Nb–O	1.94 ± 0.01	0.16	$n_{Nb-O} = 5.9_8 \pm 0.12$ $n_{O-Nb} = 1.9_9 \pm 0.04$
Li–O	2.16 ± 0.01	0.12	$n_{Li-O} = 2.7_6 \pm 0.06$ $n_{O-Li} = 0.9_2 \pm 0.02$
O–O	2.88 ± 0.01	0.58	$n_{O-O} = 7.6_0 \pm 0.15$

Table 4. Evolution of $r_{1,Nb-O}$ and n_{Nb-O} with the temperature.

Temperature (K)	$r_{1,Nb-O}$ (Å) ± 1.0%	$n_{Nb-O} \pm 5.0\%$
1490	$1.93_3 \pm 0.020$	$6.0_1 \pm 0.30$
1548	$1.93_5 \pm 0.020$	$6.0_3 \pm 0.30$
1553	$1.93_3 \pm 0.020$	$5.9_7 \pm 0.30$
1573	$1.93_8 \pm 0.020$	$5.9_8 \pm 0.30$
1623	$1.93_7 \pm 0.020$	$5.9_4 \pm 0.30$

IV,4. Discussion

Several structural features have been found: i) in the melt, the first distances, $r_{1,\mathrm{Nb-O}}$ and $r_{1,\mathrm{O-O}}$ are similar to the crystalline ones at 300 K; that is to say that NbO_6 molecules are present in the melt at high temperature without expanded Nb–O bond, ii) the first distances $r_{1,\mathrm{Li-O}}$ and $r_{1,\mathrm{Nb-Nb}}$ are also comparable to the ones observed in the crystal at 300 K; clusters are probably present in the melt with a local order similar to the crystalline one, iii) thermal expansion is observed only for the highest $r_{\mathrm{O-O}}$ distance. When applying only the usual method to the global distributions, $\mathrm{RDF}(r)_{(x)}$ or $\mathrm{RDF}(r)_{(n)}$, this last phenomenon would not be observed.

In the structures with frameworks of linked octahedra, the expansion of the solid is explained by two phenomena: the changes in shape and size of individual octahedra and the changes of tilt relative to one another. The contribution of the changes of tilt to the macroscopic expansion is considerably greater than that of changes of octahedron size. It is generally accepted that the mean edge-length thermal coefficient in an octahedron is small as long as off-centre Nb displacements are present and could become much larger when Nb becomes central, as is the case in the paraelectric phase [15]. The results of our work deny this last observation since the size of the octahedron $Nb-O_6$ defined in the rhombohedral state at 300 K is maintained in the molten $LiNbO_3$. Rigid octahedral bonds had been previously confirmed by an EXAFS study of the hydrolysis of niobium pentaethoxide [32], revealing four short Nb–O bonds (1.90 ± 0.03 Å) and two long Nb–O bonds (2.15 ± 0.03 Å); values always similar to the crystalline distances. In the melt, NbO_6 octahedra could be more regular and explain the reduction of the average Nb–O bond.

Another confirmation of the local order is obtained from the coordination numbers. The $n_{\mathrm{O-O}}$ value, nearly equal to the crystalline value, confirms the presence of NbO_6 octahedra in the melt. The $n_{\mathrm{Li-O}}$ value can be explained only if a great part of the Li atoms are bonded with three O atoms. This observation, and the fact that the value $r_{1,\mathrm{Nb-Nb}}$ is nearly equal to the crystalline value, indicate a probable presence of clusters formed by corner-shared $Nb-O_6$ octahedra tightened by lithium atoms. The evolution, observed in $G(r)_{(n)}$ around 4.53 Å when T decreases (see curves Fig. 8), is explained by an increase of the

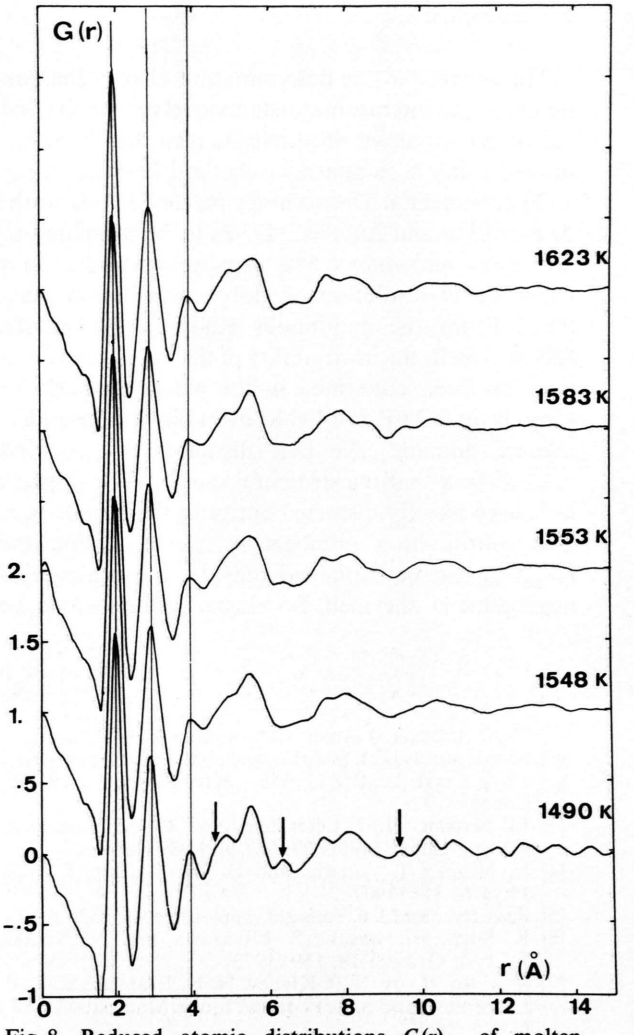

Fig. 8. Reduced atomic distributions $G(r)_{(n)}$ of molten $LiNbO_3$ (arrows indicate the most important changes in the undercooling domain).

Li–O pair contribution, a fact which confirms the previous assumption. The presence of clusters in the melt has been recently confirmed by small angle X-ray scattering [16] and the local order evolution with temperature obtained from neutron scattering [18] using samples of natural isotopic abundance. Evolution of clusters and local order have to be described more precisely to explain the high thermal expansion in a melt which contains clusters having a mean density identical to the solid one. Supplementary neutron studies are scheduled with samples having variable $^6Li/^7Li$ ratios to determine the partial structure factors $S_{ij}(Q)$.

V. Conclusion

The acuracy in the determination of coordination numbers and interatomic distances, relative to the first neighbour atoms in the $LiNbO_3$ melt, has been improved using a comparative method between X-ray and neutron data. The accuracy reached in this work: $\Delta r/r \approx 0.5\%$ and $\Delta n/n \approx 2\%$, has to be compared to $\Delta r/r \approx 1\%$ and $\Delta n/n \approx 5\%$, usually obtained from a hypothetical resolution of global distribution functions. From the continuous study in situ of the $LiNbO_3$ melt, the invariability of the n_{Nb-O} coordination has been confirmed in the whole temperature range from 1623 K to 1490 K, including a large undercooling domain. The first distances $r_{1,Nb-O}$ and $r_{1,O-O}$ show that the structural unit $Nb-O_6$ appears as a very weakly distorted entity in the liquid state. The coordination numbers n_{Li-O}, n_{O-O} and the $r_{1,Nb-Nb}$ can be explained only by the presence of aggregates in the melt. So cluster models could be described on the basis of interconnected $Nb-O_6$ octahedra with a local order similar to the crystalline one. Supplementary study is necessary to explain the large difference observed between densities of solid liquid material.

Acknowledgements

The authors gratefully acknowledge the financial support from the Special Coordination Fund for Promotion of Science and Technology granted for the "Study of the structure of clusters forming melt and its influence to the crystal growth". One of the authors, P.A., owes this work to the financial support by a S.T.A. fellowship from the Japan International Science and Technology Exchange Center. The samples were prepared in the National Institute for Research in Inorganic Materials in Tsukuba, Japan and the neutron diffraction experiments were carried out at the Institute Laue-Langevin in Grenoble, France.

[1] A. A. Ballman, J. Amer. Ceram. Soc. **48,** 112 (1965).
[2] S. A. Fedulov, Z. I. Shapiro, and P. B. Ladyzhinskii, Sov. Phys. Cryst. **10,** 218 (1965). – Kristallografiya **10,** 268 (1965).
[3] K. Nassau, H. J. Levinstein, and G. M. Loiacono, J. Phys. Chem. Solids **27,** 983 and 989 (1966).
[4] N. Niizeki, T. Yamada, and H. Toyoda, Jap. J. Appl. Phys. **6,** 318 (1967).
[5] R. L. Byer and J. F. Young, J. Appl. Phys. **41,** 2320 (1970).
[6] K. Sugii, H. Iwasaki, S. Miyazawa, and N. Niizeki, J. Cryst. Growth **18,** 159 (1973).
[7] S. A. Bol'shvov, V. P. Klyuev, N. N. Lyapushkin, A. P. Lyubimow, and S. A. Fedulov, Inorg. Materials (USSR) **6,** 824 (1969).
[8] K. Shigematsu, Y. Anzai, S. Morita, M. Yamada, and H. Yokoyama, Japan J. Appl. Phys. **26,** 1988 (1987).
[9] J. A. S. Ikeda, V. J. Fratello, and C. D. Brandle, J. Cryst. Growth **92,** 271 (1988).
[10] S. C. Abrahams, J. M. Reddy, and J. L. Bernstein, J. Phys. Chem. Solids **27,** 997 (1966). – S. C. Abrahams, W. C. Hamilton, and J. M. Reddy, J. Phys. Chem. Solids **27,** 1013 (1966). – S. C. Abrahams, H. J. Levinstein, and J. M. Reddy, J. Phys. Chem. Solids **27,** 1019 (1966).
[11] A. Smolenskii, N. N. Krainik, N. P. Kluchua, V. Y. Zhdanova, and I. E. Mylnikova, Phys. Stat. Sol. **13,** 309 (1966).
[12] Z. I. Shapiro, S. A. Fedulov, and Yu. N. Venevtsev, Inorg. Mater (USSR) **3,** 180 (1967).
[13] K. Nassau and M. E. Lines, J. Appl. Phys. **41,** 533 (1970).
[14] D. P. Birnie, J. Mater. Res. **5,** 1933 (1990).
[15] H. D. Megaw, Acta Cryst. **A 24,** 583 and 589 (1968).
[16] P. Andonov, S. Kimura, T. Sawada, and H. Kobayashi, Small angle scattering study of the liquid lithium niobate, to publish Phys. Rev. B.
[17] K. Sugiyama, K. Nomura, Y. Waseda, P. Andonov, S. Kimura, and K. Shigematsu, Z. Naturforsch. **45a,** 1325 (1990).
[18] P. Andonov, P. Chieux, and S. Kimura, J. Phys.: Condensed Matter **5,** 1 (1993).
[19] M. Maret, A. Pasturel, C. Senillou, J. M. Dubois, and P. Chieux, J. Phys. (Paris) **50,** 295 (1989).
[20] L. Koester and W. B. Yelon, The Neutron Diffraction Commission of the International Union of Crystallography. – Neutron Diffraction Newsletters (1983).
[21] V. F. Sears, Thermal neutron scattering lengths and cross-sections for condensed material research. – Report AECL 8490 (1984).
[22] H. P. Klug and L. E. Alexander, X-ray Diffraction Procedures for Polycrystalline and Amorphous Materials, 2nd ed., John Wiley & Sons, New York 1974.
[23] C. N. J. Wagner, H. Ocken, and M. L. Joshi, Z. Naturforsch. **20a,** 325 (1965).
[24] International Tables for X-ray Crystallography, Vol. 4, The Kynoch Press, Birmingham 1974.
[25] V. H. Smith, A. J. Thakkar, and D. C. Chapman, Acta Cryst. **A 31,** 391 (1975).
[26] P. Lerner, C. Legras, and J. P. Dumas, J. Cryst. Growth **3/4,** 231 (1968).
[27] T. E. Faber and J. M. Ziman, Phil. Mag. **11,** 153 (1965).
[28] W. R. Busing and H. A. Levy, Oak Ridge National Laboratory report ORNL-TM-271 (1962).
[29] D. T. Cromer and J. T. Waber, Acta Crystallogr. **18,** 104 (1965).
[30] D. T. Cromer, to suppress 1965; Acta Crystallogr. **18,** 17 (1965).
[31] M. T. Vandenborre, B. Poumellec, C. Alquier, and J. Livage, J. Non-Cryst. Solids **108,** 333 (1989).